LETTER

Adhesion Dynamics for Cellulose Nanocomposites

Niklas Nordgren,[†] Hanna Lönnberg,[‡] Anders Hult,[‡] Eva Malmström,[‡] and Mark W. Rutland*[,†]

Department of Chemistry, Surface and Corrosion Science and Department of Fibre and Polymer Technology, Royal Institute of Technology, SE-100 44 Stockholm, Sweden

ABSTRACT The efficiency of poly(ϵ-caprolactone) (PCL) as a matrix polymer for cellulose nanocomposites has been investigated at the macromolecular contact level using atomic force microscopy in a colloidal probe configuration. Model cellulose microspheres grafted with PCL were prepared via ring-opening polymerization. Force measurements between the functionalized particles revealed the adhesion to be highly dependent on the contact time because of a diffusion-controlled mechanism. Moreover, an increase of the temperature to 60 °C (close to T_m for the PCL graft) greatly enhanced the adhesion at the polymer−polymer interface, demonstrating the importance of entanglements in the annealing of composite materials.

KEYWORDS: atomic force microscopy • cellulose • surface forces • adhesion • colloidal probe • nanocomposites • ring-opening polymerization • surface grafting • poly(ϵ-caprolactone)

Cellulose, as one of the most abundant polysaccharides on earth, is highly desirable for use as a reinforcement in the production of environmentally sustainable nanocomposite materials because of the fiber's outstanding mechanical properties and inherent light weight. When cellulose fibers are dispersed in synthetic biopolymer matrixes, biodegradable nanocomposites can be manufactured. The main advantages associated with cellulose fiber reinforcement are its renewable and degradable properties in combination with low density and high specific strength (1−4). However, the limiting factor in the manufacturing of high-performance biocomposite materials is the compatibility between the fiber and the surrounding polymer matrix. Generally, when a hydrophobic polymer matrix is employed, the substantial difference in the surface energy to the fiber yields inadequate adhesion, ultimately leading to delamination (1, 2, 5). A number of studies report different ways to improve this compatibility and increase the adhesion between the matrix and fiber in the composite material (3, 6). One approach is to use native biopolymers that exhibit chemical character similar to that of cellulose. For instance, physical modifications employing either uncharged or ionic polysaccharides have shown improved adhesion between cellulose fibers. These observations have been made both macroscopically (7−9) and on the single contact level (10−13). Although some emerging enzymatic work on polysaccharide synthesis (14) is very promising, the main advantages of synthetic polymers are still the versatility and control governing the chemical composition and architecture of the macromolecules. The interfacial incompatibility in this case can be compensated for if the matrix polymer can be chemically anchored to the fiber. This can be achieved by producing covalently bound macromolecular grafts using either the "grafting-from" or "grafting-to" techniques, where the former approach facilitates direct surface-initiated polymerization and the latter refers to existing macromolecules being chemically anchored to the substrate.

Promising polymers for biocomposite applications are aliphatic polyesters, such as poly(ϵ-caprolactone) (PCL), a semicrystalline polymer that most often is obtained via ring-opening polymerization (ROP) of ϵ-CL (Figure 1) (15, 16). ROP is a controlled technique that efficiently synthesizes polymers with control over the molecular weight and enables tailoring of end groups, as well as the design of complex architectures (15, 16). Moreover, ROP can be used to polymerize monomers in situ and thereby facilitate the direct growth of polymers from a surface via the "grafting-from" approach, resulting in end-anchored polymer brushes (17−19). The "grafting-from" approach is more advantageous than the "grafting-to" approach in terms of the higher grafting density and molecular weight of the polymer brush (20, 21). These parameters have been shown to have significant effects on the interfacial adhesion (i.e., the strength and toughness) between two immiscible surfaces (22−24).

The majority of studies that have been performed in the past on improving compatibility in composite materials focus on measuring macroscopic properties, such as wetting, moisture adsorption, or the overall mechanical properties (1, 2, 6, 25−29). The direct measurements of the effects on chemical grafted cellulose composites on the single contact level have been less extensively investigated. Atomic force microscopy (AFM) in colloidal probe mode (30) has shown to be a versatile tool in quantitatively measuring the nanoscale interactions at biopolymer interfaces (12, 13).

* E-mail: mark.rutland@surfchem.kth.se.
Received for review June 2, 2009 and accepted August 31, 2009
[†] Department of Chemistry, Surface and Corrosion Science.
[‡] Department of Fibre and Polymer Technology.
DOI: 10.1021/am900381t

Published on Web 09/16/2009

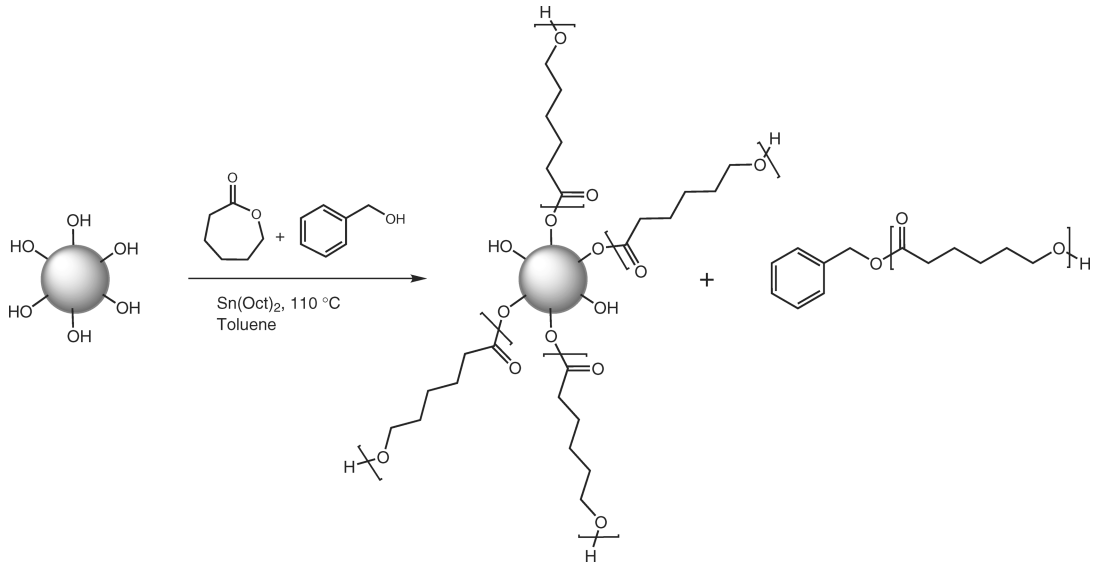

FIGURE 1. Schematic displaying the ROP procedure of surface-grafting PCL from cellulose spheres.

The successful grafting of biopolymers from cellulose using ROP (31, 32) and the resulting improvement of the macroscopic properties in composite materials have previously been reported by some of the authors (33). Although the substrates used in those studies are adequate representations of the surface chemistry of cellulose, the rather high surface roughness renders them nonideal for the quantification of nanoscale interactions using the colloidal probe AFM technique. In the present study, cellulose microspheres were employed as model surfaces. The same types of particles have previously been satisfactorily used in a range of studies by some of the authors (11−13, 34). The main goal of the present study was to elucidate the effect of grafting on the interfacial adhesion between cellulose surfaces on the nanoscopic level.

MATERIALS AND METHODS

Cellulose spheres [approximate diameters of 10 μm produced from regenerated cellulose by the viscose process (Kanebo, Japan)] were dried in a vacuum oven, at 50 °C for 24 h prior to use. ϵ-Caprolactone (ϵ-CL), benzyl alcohol, tin octoate [$Sn(Oct)_2$], toluene (p.a.), tetrahydrofuran (THF, p.a.), and methanol (MeOH, p.a.) were used as received.

Grafting of ϵ-CL via ROP. Cellulose model spheres grafted with PCL were produced via ROP of ϵ-CL using a synthetic approach similar to that in previous work (31, 32). Dried cellulose spheres (0.5 g), ϵ-CL (19.5 g, 171 mmol), benzyl alcohol (0.030 g, 0.29 mmol), and toluene (30 mL) were mixed in a single-necked flask equipped with a magnetic stirrer. To remove the majority of water in the system, 15 mL of solvent, i.e., water and toluene, was distilled off. Thereafter, the flask was sealed with a rubber septum and degassed by three vacuum/argon cycles. A catalytic amount of $Sn(Oct)_2$ (0.59 g, 3 wt % of monomer) was added to the reaction mixture under an argon flow, and the flask was then flushed for 15 min with argon. The polymerization was allowed to proceed for 4 h, at 110 °C, and the conversion of the monomer was estimated with ^{1}H NMR spectroscopy on the crude reaction mixture.

The product was dispersed in THF, after which the monomer and the ungrafted, soluble PCL were removed from the mixture via filtration. The filtrate was precipitated in methanol, and the free PCL was characterized with ^{1}H NMR spectroscopy and size-exclusion chromatography (SEC). To completely remove ungrafted PCL before surface characterization, the PCL-grafted cellulose spheres (cell-*g*-PCL) were thoroughly washed by Soxhlet extraction as well as dispersion in pure THF and filtration. The washing was complete when no PCL was detected (via ^{1}H NMR analysis) in the filtrate.

Characterization. NMR spectra were recorded at 400 MHz on a Bruker AM 400 using $CDCl_3$ as the solvent. The solvent signal was used as an internal standard.

Fourier transform infrared (FTIR) spectroscopy was conducted on a Perkin-Elmer Spectrum 2000 FTIR equipped with a MKII Golden Gate, Single Reflection ATR system from Specac Ltd., London, U.K. The spectra were normalized against a specific ATR crystal adsorption to enable a comparison between the polymer-grafted cellulose substrates (32, 35).

SEC was performed using a TDA model 301 equipped with one or two GMH_{HR}-M columns with TSK gel (Tosoh Biosep), a VE 5200 GPC autosampler, a VE 1121 GPC solvent pump, and a VE 5710 GPC degasser, from Viscotek Corp. THF was used as the mobile phase (1.0 mL/min). The measurement was performed at 35 °C. The SEC apparatus was calibrated with linear polystyrene standards, and toluene was used as flow-rate marker.

Field-emission scanning electron microscopy (FE-SEM) images were recorded on a Hitachi S-4800 field-emission scanning electron microscope. The samples were deposited on a mica plate and then mounted on a substrate with carbon tape and coated with 3 s of carbon (Cressington 108 carbon/A coater) and then 2 × 4 nm gold/palladium (Cressington 208HR sputter coater).

AFM. Force measurements and imaging were performed using a MultiMode Picoforce atomic force miccroscope with a Nanoscope III controller (Veeco; Digital Instruments, Plainview, NY) equipped with a closed-loop scanner. In this study, the colloidal probe technique (30), extended to include measurements with cellulose-functionalized probes (34), has been utilized. The measurements were conducted following the procedures extensively described in an IUPAC report (36). The PCL-grafted cellulose spheres (approximate diameters of 10 μm) were attached to the end of the cantilever using a tiny amount (~1 fL) of epoxy resin (Araldite Rapid, Casco). The cantilevers used were rectangular uncoated tipless silica cantilevers of type CSC12/NoAl (MikroMasch, Estonia) with approximate dimensions length = 90 μm and breadth = 35 μm. In order to obtain accurate normal spring constants, the cantilevers were cali-

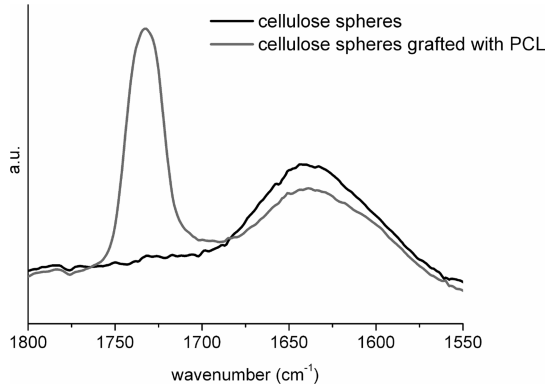

FIGURE 2. Normalized FTIR spectra of ungrafted and PCL-grafted cellulose spheres.

brated using the AFM Tune IT v2.5 software (ForceIT, Sweden), based on thermal noise with hydrodynamic damping (37−39). Additional cellulose spheres (both neat and grafted) were glued to a lower substrate (a mica sheet). Force measurements were conducted between the upper functionalized probe and the lower sphere (either neat or grafted) with a goal of elucidating the effects of the graft on the interfacial adhesion. Moreover, the effects of the contact time and temperature on adhesion were investigated (after being in physical contact at a constant normalized applied load of 14 mN/m). These parameters are of high interest for the manufacturing process of novel high-performance nanocomposite materials. Measurements were conducted in air at room temperature (20 °C) and at 60 °C. Typical force measurements were performed with a ramp size of 2 μm at a rate of 2 μm/s. The zero separation was defined by convention at a maximum applied load on approach where the cantilever deflection linearly follows the extension of the piezoscanner (the constant-compliance regime). Strictly, of course at that point the spheres have already made physical contact and undergone some deformation. Similarly, upon separation, it is difficult to sensibly define a point of zero separation because the surfaces deform under adhesive force during separation. In fact, the work required to achieve this deformation contributes to the work required to separate the surfaces, and it is therefore useful to define the zero separation in this way. (See refs 40 and 41 for a fuller discussion.) In order to verify the reproducibility, all measurements were repeated using at least three different substrates for each condition. The effective interaction radius of curvature, R, between the two interacting cellulose spheres was calculated by

$$R = \frac{R_1 R_2}{R_1 + R_2} \qquad (1)$$

where R_1 and R_2 are the radii of the two cellulose spheres.

Imaging was performed in the tapping mode at 0.5 Hz with a scan size of 2 μm × 2 μm using cantilevers of the type NSC14/AlBS (MikroMasch, Estonia).

RESULTS AND DISCUSSION

NMR and SEC analyses were used to characterize the free PCL formed in the ROP. The conversion for the ROP of ϵ-CL was estimated as 95%, and the molecular weight (M_n) was estimated as 19 700 and 28900 g/mol ($M_w/M_n = 1.9$) using ^{1}H NMR and SEC analyses, respectively. FTIR spectra of ungrafted and thoroughly washed PCL-grafted spheres confirmed the presence of covalently anchored PCL (carbonyl peak at 1730 cm^{-1}; Figure 2).

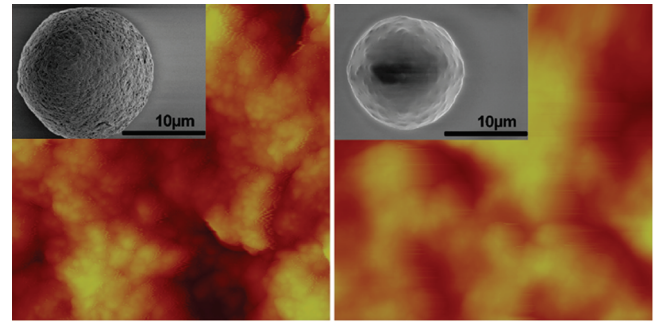

FIGURE 3. AFM tapping-mode height profiles with a scan size of 2 μm × 2 μm of ungrafted (left) and PCL-grafted (right) cellulose spheres. Insets: FE-SEM images of the ungrafted and PCL-grafted cellulose probes, respectively (diameters 10−15 μm).

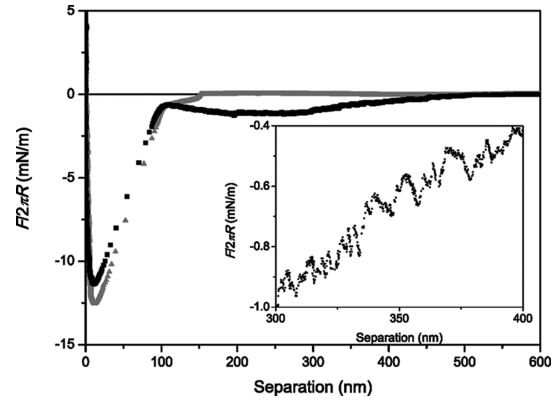

FIGURE 4. Normalized force profiles upon retraction between a PCL-grafted cellulose sphere and a neat cellulose sphere (gray triangles) and another PCL-grafted cellulose sphere (black squares). The inset shows a magnified part of the force curve between the two PCL-grafted cellulose spheres. The displayed force curves were obtained in air at 20 °C after 5 s of surface contact.

The change in the overall surface morphology of the spheres due to grafting was studied with FE-SEM, and the detailed nanoscale structure was revealed by AFM imaging. The results are displayed in Figure 3 (note that the size difference of the spheres is due to the size variations of the neat cellulose spheres used and is not an effect of the graft). As seen, the neat cellulose spheres showed a detailed surface topography, whereas the grafted cellulose spheres display the expected lower roughness due to the leveling effect of the thin polymer layer.

Adhesion Measurements. The force profiles upon retraction between a PCL-grafted cellulose sphere and a neat cellulose sphere and another PCL-grafted cellulose sphere are displayed in Figure 4. The presented force curves were obtained in air at room temperature (20 °C) after 5 s of surface contact. In both cases, the adhesion is dominated by a sharp transition with a "jump out" due to spring instability, with a range of approximately 100 nm. Under ambient conditions, this component is usually ascribed to a combination of adhesion due to van der Waals forces and any capillary forces (due to the formation of water condensates around the contact area). Detailed studies of the humidity effect on the adhesion of capillary condensates between colloidal particles (42−44) have been performed on a range of substrates, including cellulose (45, 46). This adhesive minimum is marginally smaller for the symmetric

case, probably reflecting the fact that polar contributions to the interaction are slightly smaller when a PCL layer replaces a bare cellulose surface. A striking difference between the two curves is that the adhesive forces become much more long-ranged between the two grafted surfaces. This significantly increases the work required to separate the surfaces. The reason for this improved "toughness" is the ability of the PCL chains to interpenetrate and entangle with one another across the interface. The grafted PCL chains opposing each other thus act as connector molecules (47), and the physical entanglements lead to unraveling as the surfaces are separated.

It has earlier been discussed that the separation of two spherical surfaces in contact can be likened to a crack propagation phenomenon; as the contact area shrinks during separation, the perimeter of the contact propagates analogously to a crack toward the center of the contact zone (48, 49). With this in mind, it is possible to make a direct comparison between the fracture toughness of the composites and the observed adhesion in single contacts. The bridging effect thus provides a (dynamic) additional resistance to fracture, which has been recently cited as a toughness promoter mechanism in natural biocomposites such as shells and bone via "sacrificial bonds" (50). The inset of Figure 4 displays the typical "sawtooth" pattern originating from the stretching and disruption of physical bonds as observed in earlier work for other macromolecules (10−13). By assuming that the molecular weight of the grafted polymer is comparable to the analyzed bulk polymer ($M_w = 5.49 \times 10^4$), then the extended contour length of the PCL graft can be estimated (481 repeat units × 0.875 nm/repeat unit) as 421 nm. The separation at which full detachment occurs (500 nm) corresponds at about 60% of twice the contour length (an extended chain per surface), reflecting the physical limit of the two interacting PCL grafts. Indirectly, these results also show the importance of chemical grafting (i.e., covalent linkage to the cellulose) on the adhesive toughness because the interface between the graft and the neat cellulose sphere provides a model for the adhesion strength of physisorbed PCL. This is under the assumption that the end-anchored chains have an affinity to the cellulose surface similar to that of the unconstrained polymer chains.

Figure 5 summarizes the adhesion results for the symmetric case with two opposing PCL-grafted cellulose spheres. In all cases, the magnitude of the adhesion is increased with an increase in the time for surface contact but the *range* of the force, related to the toughness, was only marginally affected under the same temperature conditions. This presumably reflects an increased number of chain penetrations with the time of contact rather than an increased penetration distance. Raising the temperature to 60 °C, which is above, or close to, the melting point of the PCL graft ($T_m = 56$ °C, obtained by DSC), greatly increases the magnitude of the adhesive force. This is not unexpected because the higher mobility of the chains results in greater entanglement between the polymer layers. The range of interaction is also significantly longer (increased toughness) than expected

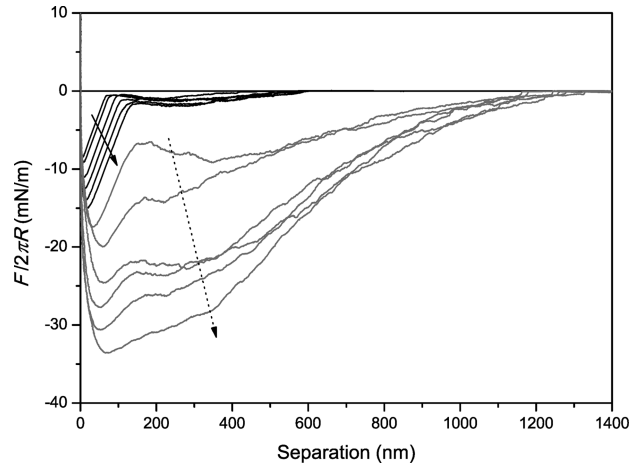

FIGURE 5. Normalized force profiles upon retraction between two cellulose spheres both bearing PCL grafts. Measurements were conducted in air at 20 °C (black curves) and at 60 °C (gray curves). The multiple curves displayed in both cases are representative measurements at increasing time of contact (0, 1, 5, 10, 30, and 100 s), as indicated by the arrows.

from the calculated contour length of the chains. We also note that the length of the graft might differ from the analyzed bulk polymer and that M_n of PCL obtained via SEC (calibrated using polystyrene standards) has shown to be considerably overestimated (15). Considering the latter, the "real" value for the contour length (of the bulk species) could be almost 50% lower. Nevertheless, because the obtained value is a mean estimate of the length, the interaction is most likely due to the entanglements of a few longer chains, possibly combined with the physical deformation of the spheres under the large adhesive force (51).

The focus of this study is on the forces on retraction (adhesion), but information can also be contained in the forces on approach, so these are briefly mentioned here. Both the symmetric and asymmetric cases at 20 °C show the same trend with a small, distinct jump (due to spring instability) into contact from around 30 nm as a result of van der Waals forces. The range of this attraction is increased up to a factor 5 for the two opposing grafts at 60 °C, indicating macromolecular-mediated bridging effects and plastic deformation. The range in this case increased slightly with longer times of surface contact, indicating some dynamic changes to the layer or the underlying cellulose. Nevertheless, because the force measurements upon retraction show full reproducibility, any permanent alteration of the layer, such as failure of either the chains or the underlying cellulose as contributing to the unexpectedly long range, can be ruled out. Finally, while it is known that a surface elastic modulus can be extracted from the contact region of the force curves (40), the modulus in this case is determined by the cellulose rather than the thin grafted film (10).

In order to quantitatively compare the effects of the graft, as well as the dynamic and temperature contributions to the adhesion, the integrated work of adhesion was calculated and plotted against the contact time (Figure 6). In all cases, the time dependence (discussed above) on the adhesion is present, but with characteristic differences depending on the conditions used. After a certain time, a plateau is reached,

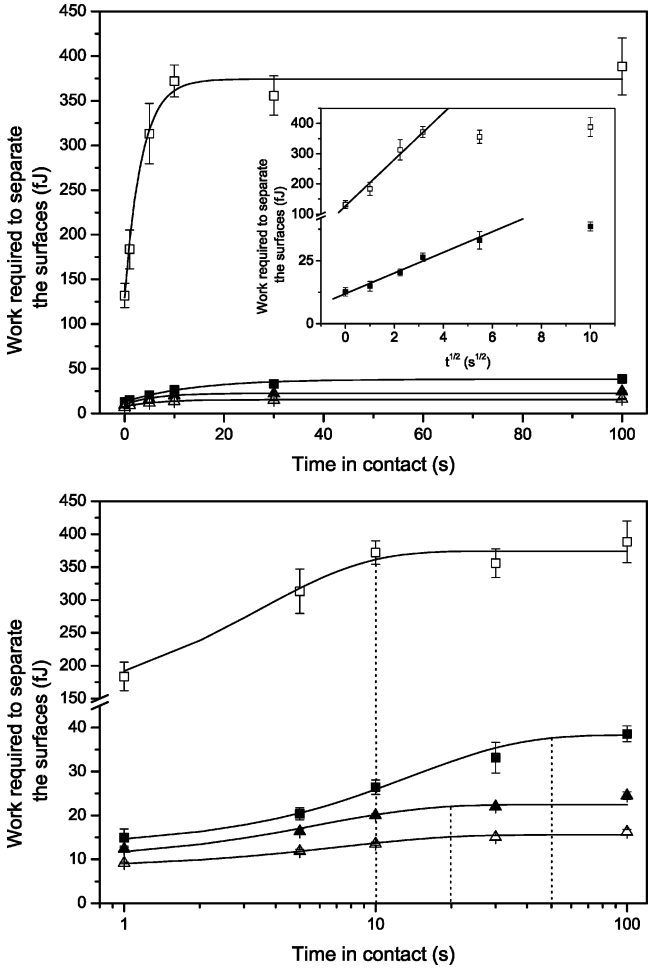

FIGURE 6. Work of adhesion as a function of the contact time on a linear scale (upper) and on a logarithmic scale (lower). The data displayed are between a PCL-grafted cellulose sphere and a neat cellulose sphere (triangles) and another PCL-grafted cellulose sphere (squares). Measurements were conducted in air at 20 °C (solid symbols) and at 60 °C (open symbols). The solid trend lines were added to guide the eye, and the dotted lines indicate the approximate onset of the plateaus. Inset: Adhesion plotted as a function of $t^{1/2}$ between two cellulose spheres both bearing PCL grafts.

which reflects the maximum adhesion obtained (on the measured time scale). From the logarithmic plot, it is obvious that the final adhesion obtained for the symmetric system (squares) is considerably higher than that for the asymmetric system (triangles) (about 50% at 20 °C). This is due to the more favorable interactions and chain entanglements when the two grafted layers are in contact. When the temperature is raised, the chain entanglement effects become more pronounced for the symmetric case as the mobility of the chains increases, resulting in an increase of the effective adhesion by a factor of 10. Interestingly, the time dependence scales with $t^{1/2}$ (see inset), which is characteristic for diffusion-like behavior (52) and has been observed earlier for other polymers (10, 53, 54). At longer time, when more entanglements are formed, theory predicts a slower ln(t) growth (52) (not reached within the experimental time scale for this study). Nevertheless, it has previously been seen that most of the interfacial toughness arises from the early stage of annealing (54, 55). Moreover, the rate of diffusion is increased at the higher temperature, which is not surprising because the chains are then in a more fluidlike regime. The asymmetric case also showed diffusion-like behavior but to a much lower extent than that between the grafted layers. Here the adhesion trend is opposite to that of the symmetric case, with a small shift of the curves to lower values at high temperature. Both the surface energy and any capillary condensation contributions to adhesion are consistent with the marginally reduced adhesion at higher T.

CONCLUSIONS

To our knowledge, this is the first time that colloidal probe microscopy has been used to evaluate adhesion and its mechanisms for bionanocomposite grafts. A major advantage of the technique is that a single contact of well-defined geometry is evaluated. The picoforce sensitivity of the technique allows highly sensitive measurements of the binding force to be made, which allows annealing times in the range of seconds to be studied. Moreover, the small applied forces mean that there is no damage to the films (the reproducibility of the measurements bears testament to this); thus, the same contact point can be evaluated repeatedly under different conditions, so very few samples need to be prepared. In conventional macroscopic approaches, a separate sample is required for each repetition of each condition measured. While it is not suggested that colloidal probe measurements will replace conventional adhesion measurements and composite fracture studies, they provide a useful screening process and require negligibly small quantities of material. Further, they provide valuable insight into the *mechanism* of adhesion. Macroscopic measurements provide a single value of the adhesion force, whereas with colloidal probe the force as a function of the negative load (or separation) is obtained. Thus, the amount of deformation of the contact, the degree of chain interpenetration, and possibly just as significantly the rate dependence of the release can all be extracted. The latter has a great deal of relevance to fracture toughness.

In this first colloidal probe investigation of cellulose surfaces bearing grafted polymers, a simple experimental matrix has allowed us to demonstrate that there is no intrinsic affinity of the PCL material for cellulose. In this case, a conventional dispersion adhesion is observed without any "chain adhesion"; i.e., the surfaces separate completely and catastrophically at a given negative load. Conversely, when the thin PCL film is chemically grafted to the surface, it is unambiguous that a diffusion-based interpenetration of the surfaces occurs, increasing adhesion and leading to a gradual release of the surfaces, occurring over a significant separation range. This indicates that not only will a nanocomposite based on this material combination be stronger but it will also be able to resist local detachment of the matrix during flexing, creep, shocking, and so on. Raising the temperature at which adhesion is measured is analogous to annealing the system, and it has been possible to quantitatively observe the increased frequency of chain interpenetrations and larger interpenetration distances, which can be related to the molecular dimensions of the graft. Forthcoming extensions

to this study will thus focus on the effects of macromolecular design (molecular weight and architecture) on the interactions. Further, friction (lateral force) is known to be intimately coupled to the interfacial adhesion (56, 57) particularly for composite materials, and this will provide another interesting avenue to pursue.

Acknowledgment. Biomime, the Swedish Center for Biomimetic Fiber Engineering (http://www.biomime.org/), and the Swedish Foundation for Strategic Research are acknowledged for financial support. AFM for this research was financed by a generous grant from the Knut and Alice Wallenberg Foundation. M.W.R. is a fellow of the Swedish Research Council.

Note Added after ASAP Publication. This paper was released ASAP on September 16, 2009. The unit description for dried cellulose spheres in the Materials and Methods section was changed and the correct version was posted on October 5, 2009.

REFERENCES AND NOTES

(1) Belgacem, M. N.; Gandini, A. *Compos. Interfaces* **2005**, *12*, 41–75.
(2) Gandini, A.; Belgacem, M. N. *Macromol. Symp.* **2005**, *221*, 257–270.
(3) Trejo-O'Reilly, J.-A.; Cavaille, J.-Y.; Gandini, A. *Cellulose (London)* **1997**, *4*, 305–320.
(4) Klemm, D.; Heublein, B.; Fink, H.-P.; Bohn, A. *Angew. Chem., Int. Ed.* **2005**, *44*, 3358–3393.
(5) Bledzki, A. K.; Gassan, J. *Prog. Polym. Sci.* **1999**, *24*, 221–274.
(6) Bledzki, A. K.; Reihmane, S.; Gassan, J. *Polym.—Plast. Technol. Eng.* **1998**, *37*, 451–468.
(7) Lima, D. U.; Oliveira, R. C.; Buckeridge, M. S. *Carbohydr. Polym.* **2003**, *52*, 367–373.
(8) Christiernin, M.; Henriksson, G.; Lindström, M. E.; Brumer, H.; Teeri, T. T.; Lindström, T.; Laine, J. *Nord. Pulp Pap. Res. J.* **2003**, *18*, 182–187.
(9) Lertsutthiwong, P.; Chandrkrachang, S.; Nazhad, M. M.; Stevens, W. F. *Appita J.* **2002**, *55*, 208–212.
(10) Stiernstedt, J.; Brumer, H., III; Zhou, Q.; Teeri, T. T.; Rutland, M. W. *Biomacromolecules* **2006**, *7*, 2147–2153.
(11) Stiernstedt, J.; Nordgren, N.; Wågberg, L.; Brumer, H.; Gray, D. G.; Rutland, M. W. *J. Colloid Interface Sci.* **2006**, *303*, 117–123.
(12) Nordgren, N.; Eklöf, J.; Zhou, Q.; Brumer, H.; Rutland, M. W. *Biomacromolecules* **2008**, *9*, 942–948.
(13) Nordgren, N.; Eronen, P.; Österberg, M.; Laine, J.; Rutland, M. W. *Biomacromolecules* **2009**, *10*, 645–650.
(14) Gullfot, F.; Ibatullin, F. M.; Sundqvist, G.; Davies, G. J.; Brumer, H. *Biomacromolecules* **2009**, *10*, 1782–1788.
(15) Biela, T.; Duda, A.; Penczek, S. *Macromol. Symp.* **2002**, *183*, 1–10.
(16) Penczek, S.; Cypryk, M.; Duda, A.; Kubisa, P.; Slomkowski, S. *Prog. Polym. Sci.* **2007**, *32*, 247–282.
(17) Husemann, M.; Mecerreyes, D.; Hawker, C. J.; Hedrick, J. L.; Shah, R.; Abbott, N. L. *Angew. Chem., Int. Ed.* **1999**, *38*, 647–649.
(18) Chen, L.; Ni, Y.; Bian, X.; Qiu, X.; Zhuang, X.; Chen, X.; Jing, X. *Carbohydr. Polym.* **2005**, *60*, 103–109.
(19) Dubois, P.; Krishnan, M.; Narayan, R. *Polymer* **1999**, *40*, 3091–3100.
(20) Fukuda, T.; Tsujii, Y.; Ohno, K. *Macromol. Eng.* **2007**, *2*, 1137–1178.
(21) Milner, S. T. *Science (Washington, D.C.)* **1991**, *251*, 905–914.
(22) Creton, C.; Kramer, E. J.; Brown, H. R.; Hui, C.-Y. *Adv. Polym. Sci.* **2002**, *156*, 53–136.
(23) Creton, C.; Kramer, E. J.; Hadziioannou, G. *Macromolecules* **1991**, *24*, 1846–1853.
(24) Sha, Y.; Hui, C. Y.; Kramer, E. J.; Hahn, S. F.; Berglund, C. A. *Mater. Res. Soc. Symp. Proc.* **1997**, *461*, 135–140.
(25) Belgacem, M. N.; Gandini, A. *Monomers, Polym. Compos. Renewable Resour.* **2008**, 385–400.
(26) Bonini, C.; Heux, L.; Cavaille, J.-Y. *Mater. Tech. (Paris)* **2000**, *88*, 55–58.
(27) Gatenholm, P.; Felix, J.; Kalson, C.; Kubat, J. *Contemp. Top. Polym. Sci.* **1992**, *7*, 75–82.
(28) Maiti, S. N.; Subbarao, R. Mechanical properties of isotactic polypropylene/wood flour composites. *International Journal of Polymeric Materials*; Taylor & Francis: London, 1991.
(29) Maldas, D.; Kokta, B. V. *Int. J. Polym. Mater.* **1994**, *27*, 77–88.
(30) Ducker, W. A.; Senden, T. J.; Pashley, R. M. *Nature* **1991**, *353*, 239–241.
(31) Lönnberg, H.; Zhou, Q.; Brumer, H., III; Teeri, T.; Malmström, E.; Hult, A. *Biomacromolecules* **2006**, *7*, 2178–2185.
(32) Lönnberg, H.; Fogelström, L.; Berglund, L.; Malmström, E.; Hult, A. *Eur. Polym. J.* **2008**, *44*, 2991–2997.
(33) Lönnberg, H.; Fogelström, L.; Zhou, Q.; Hult, A.; Berglund, L.; Malmström, E. Unpublished work.
(34) Rutland, M. W.; Carambassis, A.; Willing, G. A.; Neuman, R. D. *Colloids Surf., A* **1997**, *123—124*, 369–374.
(35) Carlmark, A.; Malmström, E. *J. Am. Chem. Soc.* **2002**, *124*, 900–901.
(36) Ralston, J.; Larson, I.; Rutland, M. W.; Feiler, A. A.; Kleijn, M. *Pure Appl. Chem.* **2005**, *77*, 2149–2170.
(37) Green, C. P.; Lioe, H.; Cleveland, J. P.; Proksch, R.; Mulvaney, P.; Sader, J. E. *Rev. Sci. Instrum.* **2004**, *75*, 1988–1996.
(38) Sader, J. E.; Chon, J. W. M.; Mulvaney, P. *Rev. Sci. Instrum.* **1999**, *70*, 3967–3969.
(39) Pettersson, T.; Nordgren, N.; Rutland Mark, W.; Feiler, A. *Rev. Sci. Instrum.* **2007**, *78*, 093702.
(40) Rutland Mark, W.; Tyrrell, J. W. G.; Attard, P. Analysis of atomic force microscopy data for deformable materials. In *Atomic Force Microscopy in Adhesion Studies*; Drelich, J., Mittal, K. L., Eds.; VSP: Leiden, 2005; pp 155—171.
(41) Attard, P.; Schulz, J. C.; Rutland, M. W. *Rev. Sci. Instrum.* **1998**, *69*, 3852–3866.
(42) Rabinovich, Y. I.; Adler, J. J.; Ata, A.; Singh, R. K.; Moudgil, B. M. *J. Colloid Interface Sci.* **2000**, *232*, 10–16.
(43) Feiler, A. A.; Jenkins, P.; Rutland, M. W. *J. Adhes. Sci. Technol.* **2005**, *19*, 165–179.
(44) Biggs, S.; Cain, R. G.; Dagastine, R. R.; Page, N. W. *J. Adhes. Sci. Technol.* **2002**, *16*, 869–885.
(45) Bogdanovic, G.; Tiberg, F.; Rutland, M. W. *Langmuir* **2001**, *17*, 5911–5916.
(46) Feiler, A. A.; Stiernstedt, J.; Theander, K.; Jenkins, P.; Rutland, M. W. *Langmuir* **2007**, *23*, 517–522.
(47) Raphael, E.; De Gennes, P. G. *J. Phys. Chem.* **1992**, *96*, 4002–4007.
(48) Maugis, D.; Barquins, M. *J. Phys. D: Appl. Phys.* **1978**, *11*, 1989–2023.
(49) Greenwood, J. A.; Johnson, K. L. *Philos. Mag. A* **1981**, *43*, 697–711.
(50) Fantner, G. E.; Hassenkam, T.; Kindt, J. H.; Weaver, J. C.; Birkedal, H.; Pechenik, L.; Cutroni, J. A.; Cidade, G. A. G.; Stucky, G. D.; Morse, D. E.; Hansma, P. K. *Nat. Mater.* **2005**, *4*, 612–616.
(51) Rutland, M. W.; Tyrrell, J. W. G.; Attard, P. *J. Adhes. Sci. Technol.* **2004**, *18*, 1199–1215.
(52) Deutsch, J. M.; Yoon, H. *Macromolecules* **1994**, *27*, 5720–5728.
(53) Plunkett, M. A.; Rutland, M. W. *J. Adhes. Sci. Technol.* **2002**, *16*, 983–996.
(54) Reichert, W. F.; Brown, H. R. *Polymer* **1993**, *34*, 2289–2296.
(55) Geoghegan, M.; Clarke, C. J.; Boue, F.; Menelle, A.; Russ, T.; Bucknall, D. G. *Macromolecules* **1999**, *32*, 5106–5114.
(56) Yoshizawa, H.; Chen, Y. L.; Israelachvili, J. *J. Phys. Chem.* **1993**, *97*, 4128–4140.
(57) Bergenstråhle, M.; Thormann, E.; Nordgren, N.; Berglund, L. A. *Langmuir* **2009**, *25*, 4635–4642.

AM900381T